JOURNAL OF AIRCRAFT
Vol. 45, No. 5, September–October 2008

Hydrogen-Assisted Fatigue Lifetime Characteristic of AF1410 Steel

A. Quispitupa,* B. Shafiq,† S. Charca,‡ and O. Uwakweh†
University of Puerto Rico, Mayagüez, Puerto Rico 00681

DOI: 10.2514/1.32172

Results of hydrogen-assisted fatigue lifetime testing indicated a substantial but gradual increment in crack growth rate as a function of increasing hydrogen content. Hydrogen was introduced into both sides of the specimen simultaneously via galvanostatic charging. Extensive scanning electron microscope fractographic analyses revealed a clear shift in the modes of failure and changes in fracture surface morphology as a function of increasing hydrogen content. A methodology is outlined that can be used to predict fracture surface features as a function of applied stress intensity factor. A convenient deterministic model is proposed that seems to reasonably accurately capture the crack growth rate behavior under strain controlled testing conditions. In addition, successful application of acoustic emission technique to classify various cracking stages in full spectrum testing was performed on hydrogen charged samples.

I. Introduction

IT IS generally agreed that the deleterious effects of environment in high-strength steels under stress mainly stem from the environmental hydrogen that is electrochemically produced as a result of certain reactions between the metal surface and the environment [1,2]. The effects of hydrogen in steels have been extensively studied; however, literature is mostly limited to static loading scenarios [3,4]. Under corrosion fatigue, quantifying the rate of production, ingress and/or diffusion, and retention of the environmentally produced hydrogen into the metal surface at the tip of a growing crack is in general not possible [2]. Consequently, the existing empirical and analytical fatigue lifetime prediction methodologies have enjoyed only a very limited success, especially when environmental factors are involved, due mainly to lack of significant crack tip electrochemical/micromechanical data on one hand and a deterministic relationship between parameters of interest on another [1,2].

Analytical fatigue lifetime models based on hydrogen diffusion concepts seek to establish a functional relationship between various intrinsic and extrinsic parameters, such as applied stress, rate of diffusion, and accompanying electrochemical parameters in the form of a system of partial differential equations along with complex boundary conditions, as typified by Eq. (1), for example [2]:

$$\frac{\partial C}{\partial t} = D\nabla^2 C + \nabla\left(-\frac{DC}{RT}V_H \nabla\sigma_{kk}\right) - \frac{\partial C_r}{\partial t} - \frac{\partial C_i}{\partial t}$$
$$J = -D\cdot\nabla C - \frac{DV_H}{RT}C\nabla\sigma_{kk} \tag{1}$$

where D, C, V_H, σ_{kk}, R, T, C_r, and C_i refer to diffusion coefficient, hydrogen concentration, partial molar volume of hydrogen atoms, hydrostatic stress, gas constant, absolute temperature, reversible trapped hydrogen concentration, and irreversible trapped hydrogen concentration, respectively. Analytical elasto-plastic solutions have also been attempted that seek to relate the extent of hydrogen diffusion and crack growth mechanisms, such as shown in Eq. (2) [2]:

$$\frac{2(1+\upsilon)K_\rho}{3\sigma_{ys}(2\pi)^{1/2}} = \chi_{cr}^{1/2}\left[\ell_n\left(1+\frac{\chi_{cr}}{\rho}\right)+\frac{1}{2}\right] \tag{2}$$

where K_ρ, ρ, υ, and σ_{ys} refer to stress intensity factor, notch-root radius, Poisson ratio, and yield strength, respectively. χ_{cr} signifies the critical distance ahead of the crack tip where hydrostatic stresses achieve a maximum value and hydrogen concentration is assumed to become critical [5]. A rigorous and cumbersome analytical/numerical solution [of Eqs. (1) and (2)] generally yields the rate of crack growth as a function of applied stress and hydrogen content [6,7]. However, in spite of the closed and deterministic form of the analytical solutions, the results seldom match actual service lifetime behavior of steel components due to various crack tip microstructural and electrochemical unknowns. On the other hand, empirical (Paris-type) relationships as shown in Eq. (3) can not truly be qualified as lifetime predictive tools, as they are all essentially based on curve fitting and thus fit the data well as long as the equation constants are properly adjusted.

$$\frac{da}{dN} = C(\Delta K)^m \tag{3}$$

As a result, analytical and empirical approaches have never gained broader success in predicting fatigue lifetime of materials. However, various modified forms of semi-empirical relationships that seek to establish a phenomenological relationship between physical parameters, material, and cracking behavior have proven to be more robust in their practical use than the purely analytical or purely empirical predictive models [8]; one such model is developed and proposed in this paper.

Discerning causes of failure is crucial in fatigue analysis, and scanning electron microscope (SEM) analyses have become the tool of choice for the forensic postfailure deductions [3,6–8]. It has been proposed that hydrogen diffuses into the lattice just ahead of the crack tip and aids in the embrittlement of the alloy, leading to shifts in the fracture modes and resulting lifetimes [2,3,9]. However, during routine operation, the damage induced by environmental hydrogen is not easy to account for because the material remains apparently undamaged and cannot be detected by classical inspection methods [10,11]. The nondestructive acoustic emission (AE) technique has been found to be a useful technique for conducting in situ monitoring of critical failure events that may otherwise be missed [12,13]. However, deciphering fatigue induced AE data can be a complex and challenging process as the output is a mixture of multitude of minute and erratic low energy cracking signals mixed with various sources of

Received 15 May 2007; revision received 8 November 2007; accepted for publication 18 December 2007.

*Currently Post-Doctoral Fellow, Technical University of Denmark.
†Professor, Department of Engineering Science and Materials, School of Engineering, Box 9044.
‡Graduate Student, Department of Civil Engineering, School of Engineering, Box 9041.

background noises [13–15]. Therefore, the successful implementation of AE technique requires substantial preliminary calibration, parameter adjustment, and threshold setups to filter out the undesirable signals while retaining the meaningful AE data [13–15].

The current test program examined scarcely studied ultrahigh-strength AF1410 alloy that has been used in some of the Navy's F-18E arresting shanks [1,16] to 1) study and model the hydrogen concentration effect on fatigue crack growth behavior and 2) evaluate the applicability of acoustic emission technique to monitor the fatigue crack initiation and growth processes in hydrogen charged specimens. An expected outcome is a reasonably good data along with a viable predictive model that aid in the operationally safe lifetime prediction of the ever-increasing carrier based aging aircraft fleet of the navy.

II. Experimental Setup

AF1410 steel is a secondary hardening, martensitic steel with retained austenite that combines high hardness and strength with exceptional ductility and toughness (strength $\sim$1.8 GPa and toughness $\sim$130 MPa $\cdot$ m$^{1/2}$). Experiments were intended to simulate the hydrogen produced when aircraft steel components are subjected to service in the marine environment. However, even when production of hydrogen due to interaction with the marine environment can be estimated with innovative techniques, it is nearly impossible to accurately estimate the rate of diffusion and retention of hydrogen into the material [16–19]. Therefore, to develop a fair quantitative understanding of the effects of hydrogen, specimens were electrochemically charged. For the first set of testing, compact tension (CT) specimens were charged on both sides under simultaneous galvanostatic polarization at $i_c = 2$ mA/cm^2 in a controlled manner from 0 to 84 h, which introduced various levels of hydrogen concentrations (penetration depths) as shown in Fig. 1. Strain controlled fatigue testing was conducted at room temperature on CT specimens of dimensions $5 \times 4 \times 0.32$ cm at a frequency of 0.5 Hz, strain ratio of 0.3, and at $\sim$26% of the ultimate quasi-static strain with an initial K $\sim$ 32 MPa $\cdot$ m$^{1/2}$ [20].

A second set of testing included tension-compression loading performed on hydrogen charged flat rectangular specimens of dimensions $12 \times 2.8 \times 0.15$ cm with a central hole of 6.35 cm. Testing was performed at a stress level of 33% of ultimate (tension and compression) under triangular waveform load control at a frequency of 1 Hz. Because the hydrogen charge has a tendency to escape from the metal surface, it is difficult to know the precise amount of hydrogen at any given instant during the fatigue testing period; this represents a significant limitation [1–3]. To obtain meaningful data, various precautionary/preliminary measures were considered: 1) several tests were performed to determine the fatigue life as a function of free hydrogen desorption (FHD) time (Fig. 2), 2) testing was conducted at a substantially high stress level to reasonably minimize testing time and optimize the presence of hydrogen, and most importantly 3) charging and testing were synchronized based on the FHD process curve shown in Fig. 2. For example, the first sample was charged for 35 min and complete failure occurred in 670 s under the fatigue loading; therefore, the second sample charged for 35 min was subjected to fatigue testing after 670 s (FHD time) (Fig. 2). Similarly, the second sample lasted 2050 s; therefore, the time of testing of third sample was adjusted based on the FHD curve to start where the second test ended. In this manner, it is expected that a full spectrum of fatigue life as a function of amount of hydrogen has been obtained.

For the second set of testing, AE setup was used to monitor the cracking behavior. A sketch of the AE system with two picosensors used in a linear array on the flat rectangular specimen surface at 30 m distance from each other is shown in Fig. 3. ASTM E976 standard lead breaks of 0.5 mm diameter and 2 H of hardness were used to calibrate the AE system and source location parameters [13]. To minimize extraneous background and frictional noise, high damping rubber was used around the loading pins, whereas a threshold value of 35 dB and filtering frequency of 10–1000 kHz were established. After significant preliminary testing and data processing, 20 dB was found to be the most suitable preamplifier parameter, whereas the AE software control system used 40 dB of preamplifier [10–13].

Finally, a JEOL JSM 6100 scanning electron microscope operated at 20 kV, 20-mm working distance, and 1 mm aperture was used to enhance the depth of field of the SEM images. SEM secondary electron images of the fracture surfaces helped to understand failure mechanisms and shifts in the modes of failure due to hydrogen effect [3,9,21].

III. Experimental Results

A. Hydrogen Concentration

Fatigue test results for CT specimens indicated a sharp but gradual decrease in the lifetime accompanied by a shift in the modes of failure from ductile to brittle as a function of increasing hydrogen content, as

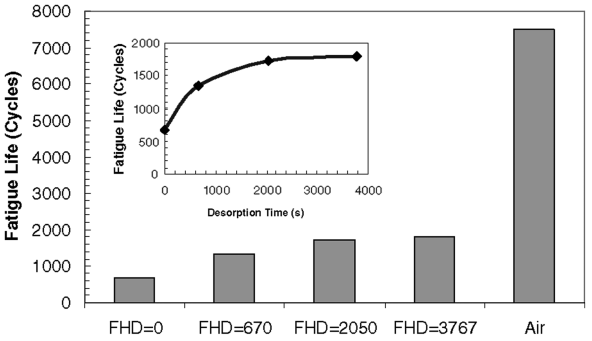

Fig. 2 Tension/compression fatigue life with prior hydrogen charging of 35 min at various desorption times.

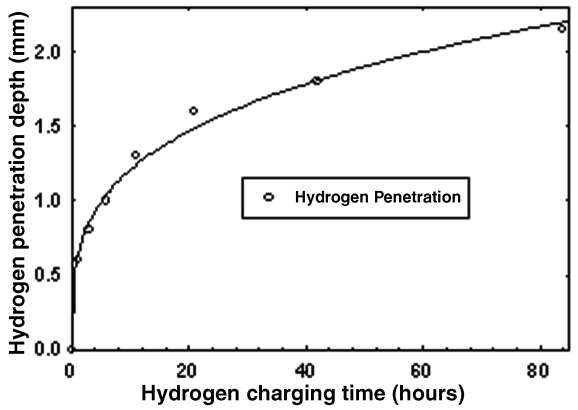

Fig. 1 Hydrogen penetration depth as a function of hydrogen charging time.

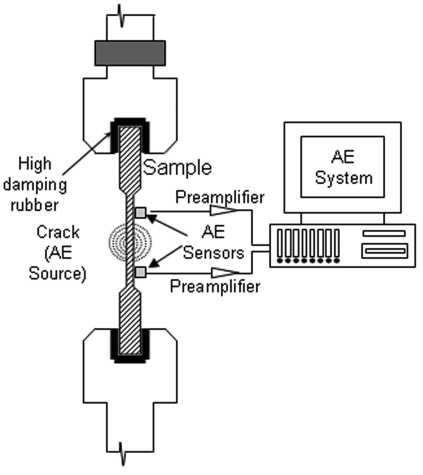

Fig. 3 Acoustic emission setup for flat rectangular specimens.

shown in Fig. 4, with the results agreeing well with the reported literature [2,5,9]. Similarly, flat rectangular samples exhibited drastic reduction in the fatigue lifetime due to prior hydrogen charging, whereas fatigue life had a decreasing trend as a function of decreasing FHD time, as indicated in Fig. 2.

B. Acoustic Emission

The resulting AE activity due to fatigue failure events was divided into three stages viz. 1) stage 1 with high AE activity that corresponded to crack initiation process, 2) stage 2 yielded very low activity levels that corresponded to stable crack growth, and 3) stage 3 was the onset of catastrophic failure revealed by maximum levels of AE activity (Fig. 5). Figure 5 also shows a rising AE activity as a function of increasing FHD time (i.e., with decreasing hydrogen content). As compared with specimens tested in air or in the presence of NaCl electrolyte, the resulting AE activity was observed to be higher in hydrogen charged samples due mainly to the presence of multiple secondary cracks as shown in the SEM images in Fig. 6.

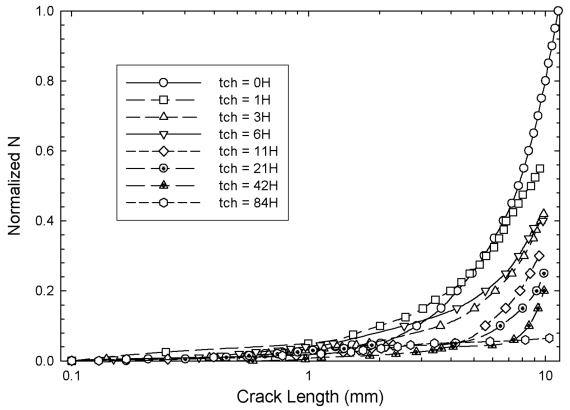

Fig. 4 Experimental results for different hydrogen charging times as a function of number of cycles.

C. SEM Observations

Typical SEM images shown in Fig. 7 clearly indicate a shift in the modes of failure as a function of increasing hydrogen content into the steel specimens. The hydrogen-induced weakening of grain boundaries resulted mainly into intergranular (IG) or quasi cleavage (QC) brittle features, whereas mainly microvoid ductile features were observed in the regions devoid of hydrogen.

IV. Discussion of Results

A. Hydrogen Concentration Effect

In general terms, the contrast in lifetime behavior between hydrogen charged and uncharged specimens pointed to loss of coherency (between the dispersed particles and matrix) and brittle behavior in the first case and competing mechanisms of strengthening due to fine particle-matrix coherency and strain hardening followed by reduced dislocation mobility in the latter. The phases present in AF1410 steel include ferrite (body centered cubic crystal structure), lath martensite (body centered tetragonal crystal structure), small fraction of retained austenite ~3% (face centered cubic crystal structure), bainite, and carbide precipitates such as $(MoCr)_xC$ [9,16]. Each of these has its relative abilities to retain reversible and irreversible atomic hydrogen. The fatigue behavior of uncharged samples and relatively longer lifetime observed in Figs. 2 and 4 an be explained from the combination of factors such as toughening due to austenitic to martensitic transformation that was strain induced [16,22]. Consequently, the shorter fatigue lifetime of hydrogen charged specimens could be explained by the absence or elimination of austenitic to martensitic transformation as a toughening mechanism due to likely prior hydrogen-induced transformation of some of the retained austenite because the steel is heavily alloyed, or the stabilization of the austenitic phase due to solid solution solute interaction with hydrogen that can lead to macroscopic ductility caused by hydrogen embrittlement [2,3,6,23]. Additionally, as a result of AF1410 age hardening (950 ± 10°F) the precipitation agent produces very fine $(MoCr)_2C$, which generally are of the coherent types, finely dispersed and well bonded to the matrix and yielding the best microstructures for combining

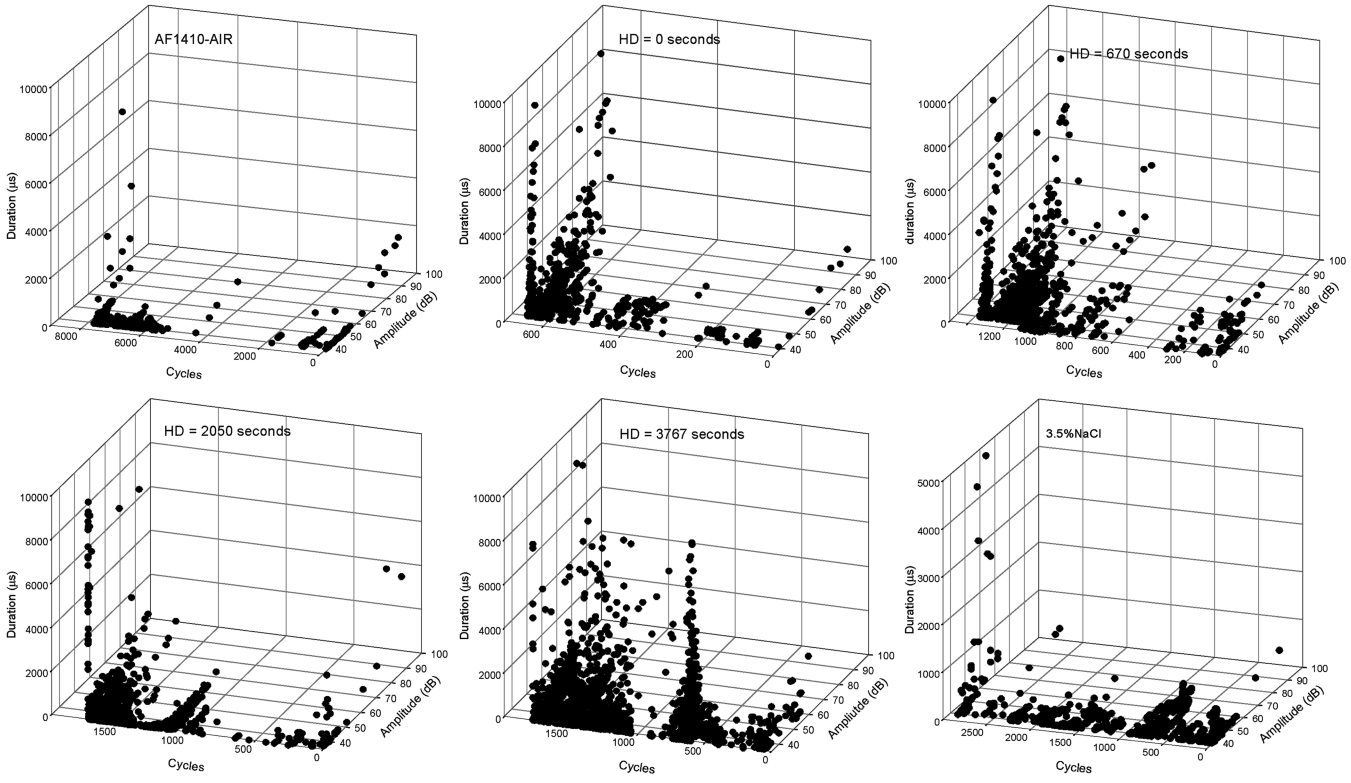

Fig. 5 AE activity in a tension/compression test in air at various FHD times and a specimen tested in the presence of 3.5% NaCl (simulated marine environment) for comparison.

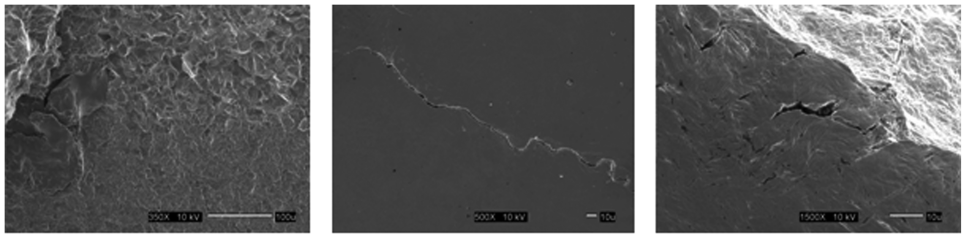

Fig. 6 SEM images of typical fracture surface morphology.

toughness with strength [9,16,22]. In other words, if the interfaces between the particles and the matrix were of the coherent type, then microvoid formation by decohesion will be avoided or made difficult; this would be lost when hydrogen is attracted to the coherent interface because decohesion would result. On the other hand, prevention of overlap of stress field with well-dispersed nonfine particles (which is the cause of enhanced mechanical properties of the AF1410 alloy) will fail when hydrogen is present. Presence of hydrogen can also cause overlapping stress field with nonspherical and nonequiaxed particles because the particle edges will act as stress concentration raisers. Needless to say, presence of hydrogen in these cases would exacerbate failure as multiple pileup of dislocation of hydrogen atmospheres would result [20].

B. Hydrogen-Assisted Fatigue Crack Growth Model

To quantify the effect of hydrogen concentration on fatigue crack growth rates, a semi-empirical crack growth model was developed that seeks to avoid the complexities involved in the existing analytical and empirical fatigue lifetime predictive methodologies. The model incorporated several relevant intrinsic (Young's modulus, yield stress, ultimate stress, etc.) and extrinsic (frequency, environment, crack length, hydrogen concentration, etc.) parameters to enhance its predictive capabilities [8]. The model introduced an effective thickness that reflects the hydrogen concentration within the material, as indicated in Eq. (4):

$$t_{\text{eff}} = t - t_{\text{HP}} \tag{4}$$

where t is the specimen thickness, and t_{HP} refers to experimentally obtained hydrogen penetration depth represented as

$$t_{\text{HP}} = (15.3 t_{\text{ch}} D)^{0.5} - 3.5t\left(\frac{t_{\text{ch}} D}{t^2}\right)^{0.72} \tag{5}$$

where t_{ch} stands for hydrogen charging time and D is the coefficient of hydrogen diffusion. The first term of Eq. (5) was obtained based on permeation breakthrough time, which reflects the maximum penetration depth of hydrogen in an ideal (theoric) material, which did not correspond to the material at hand. A second term was therefore incorporated to correct the actual hydrogen distribution depth as function of material thickness, coefficient of diffusion, and charging time. The constants of the second term depend on the electrolyte used for charging.

Using Eqs. (4) and (5), along with various mechanical and environmental intrinsic and extrinsic parameters, a fatigue lifetime relationship between number of cycles and crack length was developed, as given in Eq. (6):

$$N = \frac{\pi E a^{\left(\frac{t_{\text{eff}}}{t}+1+\upsilon\right)}}{\sigma_{\text{ys}}} + \frac{4\sigma_u a}{\left(\frac{t-t_{\text{eff}}}{C_1}\right)^{\upsilon/C_2} + 1} \tag{6}$$

where N, a, E, α_{ys}, σ_u, and υ refer to number of cycles, crack length (mm), young modulus (MPa), yield strength (MPa), ultimate tensile strength (MPa), and Poisson's ratio, respectively, whereas $C_1(=0.62)$ and $C_2(=0.28)$ were obtained from the potential regression curve. Finally, using Eq. (6), the crack growth rate model is expressed by the following expression:

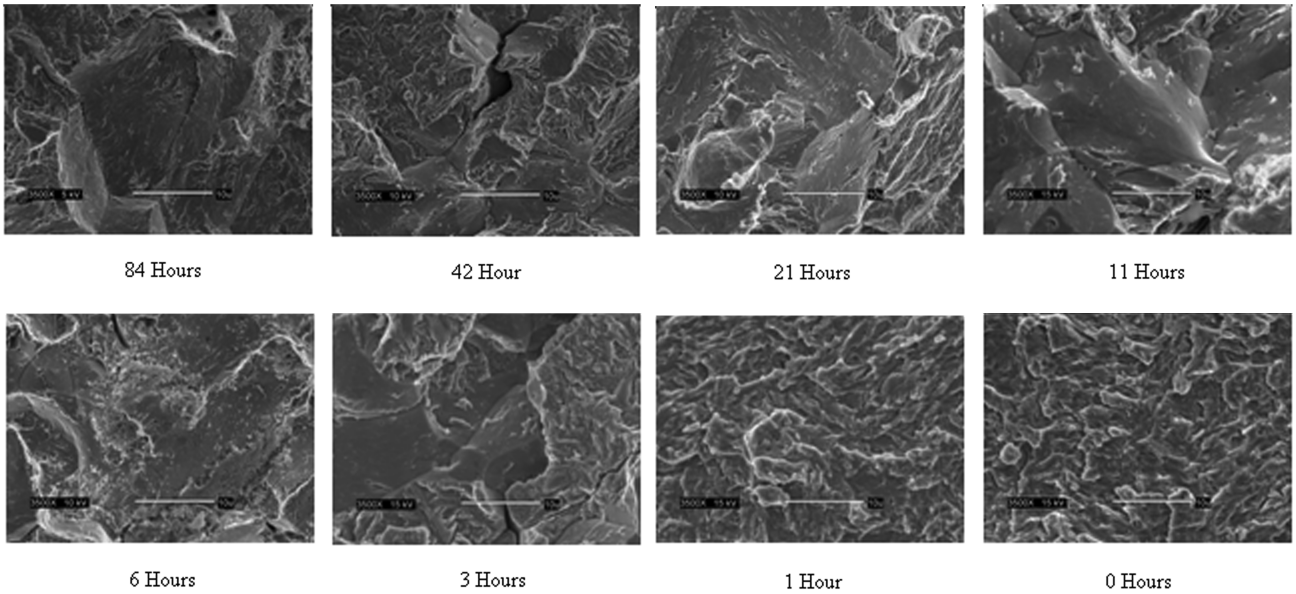

Fig. 7 SEM fracture surface images taken at ∼1 mm from the precrack length (3500X) for various hydrogen charging times (0–84 h) revealing the shifts in fracture mode due to increasing hydrogen content.

$$\frac{da}{dN} = \left[\pi \cdot E \cdot a^{\left(\frac{t_{\text{eff}}}{t}+\upsilon+1\right)} \cdot \frac{\left(\frac{t_{\text{eff}}}{t}+\upsilon+1\right)}{a \cdot \sigma_{\text{ys}}} + \frac{4 \cdot \sigma_u}{\left(\frac{t-t_{\text{eff}}}{C_1}\right)^{\upsilon/C_2}+1}\right]^{-1} \tag{7}$$

Using Eq. (7), Fig. 8 offers an example of predicted fatigue lifetimes of CT specimens charged to various levels of hydrogen and indicating a good fit with the experimental data. The small variations observed in Fig. 8 between the experimental and predicted plots may have resulted as microstructural/phase changes were not implicitly involved in the formulation of the model and/or due to the random distribution of the hydrogen into the material and perhaps due to the presence of material imperfections/dislocations that could accelerate or impede the crack propagation.

The main attraction of this model is that it is easy to implement and physically sound as it incorporates various relevant physical parameters in its development. For instance, the experimental curve fitting is kept to an absolute minimum, yet the model remains very convenient to apply, and is devoid of complexities involved in the analytical solution of simultaneous PDEs. The model can also be applied for the fatigue lifetime assessment of specimens subjected to corrosive (marine) environments. However, a limiting aspect in such problems is the inaccurate crack tip hydrogen content estimation (resulting from electrochemical reactions) and its subsequent concentration/penetration depth assessment.

C. Acoustic Emission

A combination of AE signals originating from regions rich in hydrogen (with mainly brittle fracture behavior), from the interface (with mixed ductile-brittle behavior) and from regions devoid of hydrogen (with predominantly ductile fracture behavior) were observed during fatigue testing of flat tension-compression specimens. This combination of AE signals emitted by the material was caused by asymmetric hydrogen charging that generated varying hydrogen concentration profiles into the specimen causing mixed fracture modes. Since AF1410 steel possesses a highly dislocated lath martensite, it is expected that due to hydrogen presence, the dislocation emission and mobility increases at high stress regions.

During stage 1, or crack initiation period, the sources for AE signals activity were produced mainly by internal material accommodation, friction, and dislocation-microstructural rearrangements [13–15]. The presence of hydrogen also generates a greater number of microcracks as compared with specimens tested in air, which coalesces to create macrocracks leading to shorter crack initiation times, which was reflected by the AE data shown in Fig. 5. Sources of AE signals also included a large number of secondary surface cracks (as shown in Fig. 6) on the lateral surface, where hydrogen charging was performed. However, the energy levels of secondary cracks were too low to be properly picked up and classified.

During stage 2, or stable crack growth regime, multiple secondary cracks but fewer surface cracks were observed as compared with stage 1. This behavior was attributed to the volume of the material being stressed. The stresses at a crack tip were higher than stresses around the hole; however, the volume of material due to the presence of the hole was larger than at the crack tip. Therefore, higher AE activity was observed at the initial part of the testing, which corresponded to the amount of the material being stressed. In both hydrogen charged and uncharged samples, the AE behavior observed in Fig. 5 corresponded to the material's progressive failure that consisted of microcracking, cyclic crack incubation, gradual formation, and eventual crack propagation. This behavior was observed throughout the crack initiation and stable crack growth regime. Frequent periods of crack growth dormancy were also noticed, with longer periods of dormancy corresponding to samples tested in air. Catastrophic failure occurred during stage 3, accompanied by highest levels of AE energy and amplitude, as seen in Fig. 5.

The results of tests performed on uncharged specimens yielded longer fatigue lifetimes, ductile behavior, and lower crack growth rates, which also corresponded to low AE activity as observed in Fig. 5. The amplitudes of AE signals for typical ductile cracking were low compared with brittle fracture modes, which agreed with the literature [15]. The low energy levels were also corroborated by the SEM analysis that revealed a typical flattened-microvoid ductile fracture mode for uncharged specimens, as seen in Fig. 9.

However, it was not possible in general to relate failure modes (such as intergranular, transgranular, microvoids, etc.) to AE energy and amplitude, primarily because of a significant mismatch in the AE activity and energy levels of such events and major cracking events. Filtering and threshold setups needed to eliminate undesirable background/machine noise apparently also obscured minute AE activity levels corresponding to cracking micromechanisms, which represents a limitation of the AE technique, especially during postfailure analysis. Furthermore, even though AE technique permitted in situ information of the failure events, in high-strength alloys, the sources of such activity become so diverse and out of range of each other that even with proper setup and vigilance, it becomes a challenge to retain all useful data without obscuring some critical events.

D. SEM Fracture Surface Analyses

The occurrence of pure brittle IG fracture could in general be attributed to the ability of grain boundaries to act as a hydrogen trapping sites that serve to reduce the grain boundary strength [6,9,23]. On the other hand, quasi-cleavage (QC) features that were mainly observed in specimens with higher hydrogen concentration (charging time over 3 h in the current case) can be produced as a result of metal and hydrogen atoms' interaction causing the alignment of some crystallographic planes/dislocations in the weak direction between grains. Cleavage or QC features in the host metal can also occur as hydrogen degrades cohesive forces by occupying interstitial sites in the metal lattice thus causing an increase in the lattice volume and inducing internal stresses along specific crystallographic planes (cleavage planes) [22,23]. The occurrence of IG or QC features depends on the relative strength of both the grain boundary and the metal lattice; however, the probability of occurrence of QC mode increases as hydrogen concentration increases in the host metal.

Hydrogen diffusion is in general a function of specimen thickness; therefore, the amount of hydrogen decreases almost exponentially from the specimen surface to the midplane. As a result, MV ductile type features were observed mostly in the central regions of the specimen, as evidenced by the typical low magnification SEM image shown in Fig. 9. In contrast, at the interface between the regions affected by hydrogen and devoid of hydrogen, a combination of fracture modes such as brittle IG, TG, QC, ductile TG, and MV features can be observed (Fig. 9).

The SEM fracture surface analyses and results were summarized to construct Fig. 10, which can be used to qualitatively predict the expected failure mode for hydrogen charged specimens as a function of applied stress intensity factor. Figure 10 indicates that under strain controlled testing, the expected fracture mode passes from brittle TG and QC to IG. Notice that TG and QC features predominantly occur at intermediate stress intensity factors, whereas IG fracture modes occur at low stress intensity factor, which also coincides with the threshold level for crack initiation [3]. Figure 10 serves for both K rising (load control) and K decreasing (strain control) testing as indicated by the arrows shown and outlines a convenient methodology for failure mode prediction; however, the procedure is found to be somewhat sensitive to testing mode and applied stresses.

V. Conclusions

The testing program was devised to understand the effect of hydrogen concentration on the crack growth rate behavior of ultrahigh-strength (AF1410) steel. The results indicated a significant jump in the crack growth rate as the level of hydrogen concentration increased. The effects of hydrogen were discussed in light of the microstructural aspects of the studied multiphased material. A semi-empirical model was proposed, which is expected to be useful and relevant in the fatigue lifetime prediction due to its combined

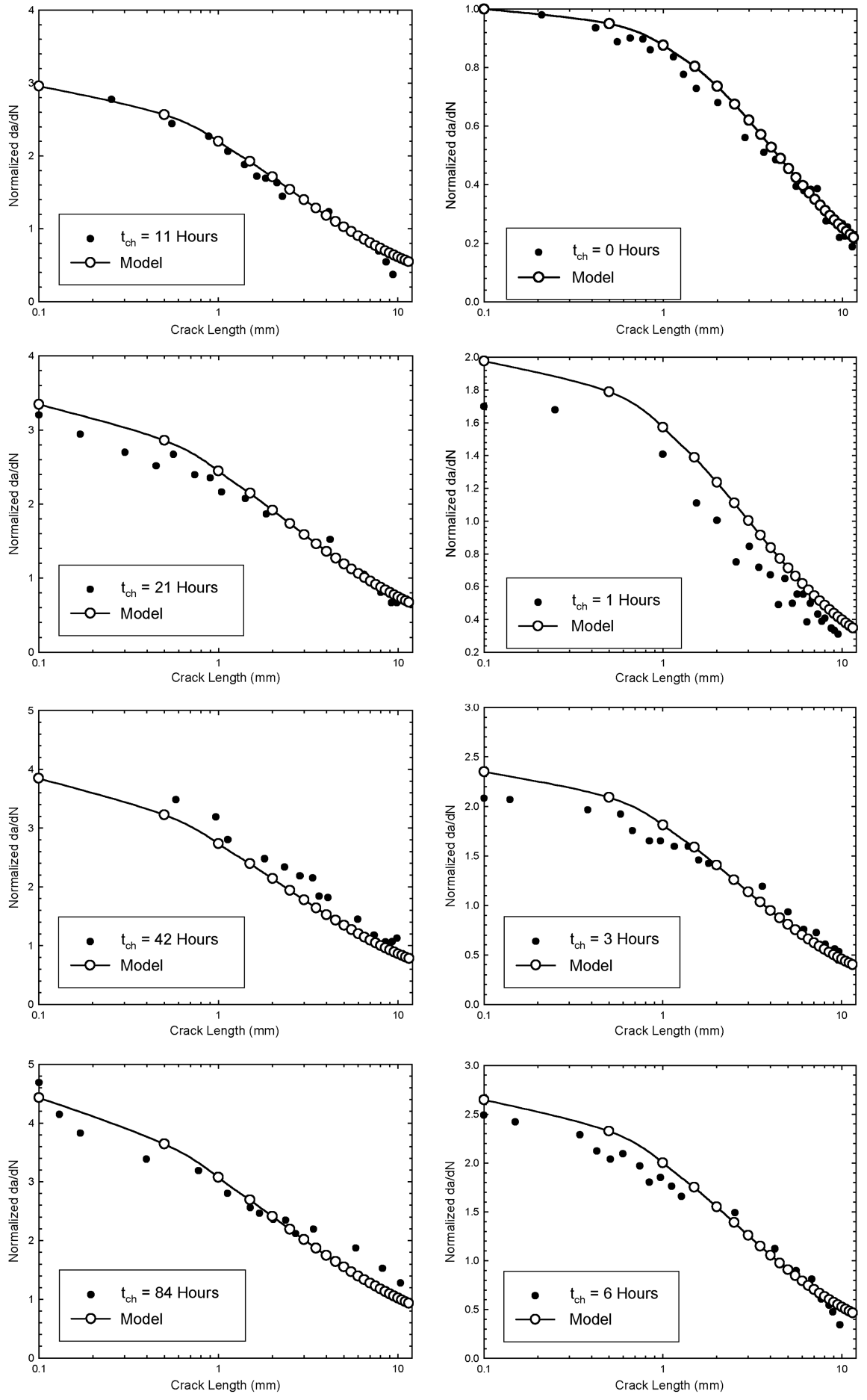

Fig. 8 Crack length versus crack growth rate at different hydrogen charging times.

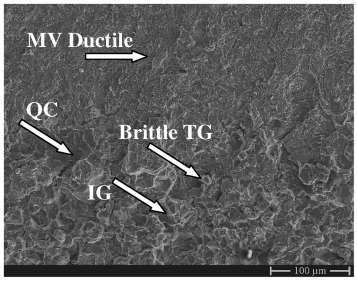

Fig. 9 Fracture surface at regions with and without hydrogen. Brittle IG, TG, QC, and MV ductile modes can be observed.

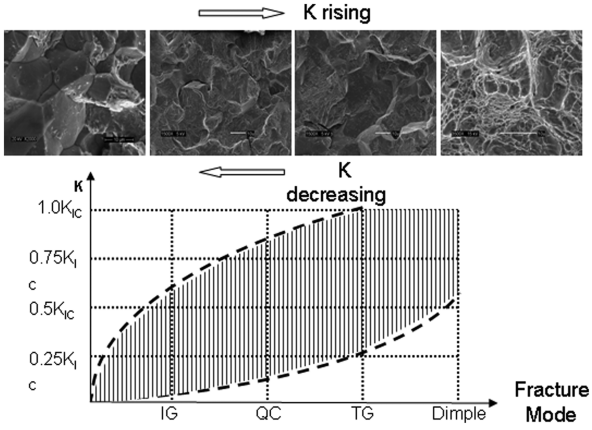

Fig. 10 Qualitative fracture mode identification for hydrogen charged samples as a function of the applied stress level.

robustness and simplicity. The model incorporated various relevant fatigue crack growth parameters in its development and fitted the current data within 5% accuracy in most cases. Finally, AE technique was found to be a practical tool for continuous monitoring of the fatigue lifetime, however limited to major failure events. Rigorous SEM analyses indicated a transition from ductile to brittle modes with the introduction of hydrogen.

Acknowledgments

The authors wish to acknowledge Yapa Rajapakse, the Office of Naval Research (ONR) program manager, and Vinod Agarwala of ONR Global for their support and guidance. The authors also wish to thank O. M. Suarez for his constructive comments and help.

References

[1] Quispitupa, A., Shafiq, B., Suárez, O., Uwakweh, O., and Duque, N., "Corrosion Fatigue of High-Strength Aircraft Structural Alloys," *Journal of Aircraft*, Vol. 43, No. 3, 2006, pp. 787–792. doi:10.2514/1.17296

[2] Turnbull, A., "Modeling of Environment Assisted Cracking," *Corrosion Science*, Vol. 34, No. 6, 1993, pp. 921–960. doi:10.1016/0010-938X(93)90072-O

[3] Beachem, C., "New Model for Hydrogen-Assisted Cracking (Hydrogen Embrittlement)," *Metallurgical Transactions*, Vol. 3, Feb. 1973, pp. 437–451.

[4] Charca, S., Uwakweh, O., and Agarwala, V., "A. Hydrogen Transport in Cathodically Polarized AF1410 Steel: Hydrogen Transport Conditions and Effects," *NACE Tri-Service Corrosion Conference Session on Corrosion Mechanisms and Kinetics*, Nov. 2005.

[5] Nagumo, M., "Function of Hydrogen in Embrittlement of High-Strength Steels," *ISIJ International (1989) (Iron and Steel Institute of Japan)*, Vol. 41, No. 6, 2001, pp. 590–598. doi:10.2355/isijinternational.41.590

[6] Thompson, A., and Bernstein, I., "Stress Corrosion Cracking and Hydrogen Embrittlement," *Metallurgical Treatises*, edited by J. K. Tien and J. F. Elliott, The Metals Society–American Institute of Metallurgical Engineers, Warrendale, PA, 1981, pp. 589–601.

[7] Gangloff, R., "Critical Issues in Hydrogen Assisted Cracking of Structural Alloys," *Environment Induced Cracking of Metals (EICM-2)*, 1st ed., edited by S. Shipilov, R. Jones, J. Olive, and R. Rebak, Elsevier, Oxford, England, U.K., 2005, ISBN 0080446353.

[8] Bailon, J., and Antolovich, S., "Effect of Microstructure on Fatigue Crack Propagation: A Review of Existing Models and Suggestions for Further Research," *Fatigue Mechanisms: Advances in Quantitative Measurement of Physical Damage, ASTM STP 811*, edited by J. Lankford, D. L. Davidson, W. L. Morris, and R. P. Wei, American Society for Testing and Materials, Philadelphia, PA, 1983, pp. 313–349.

[9] Thomas, R., Scully, J., and Gangloff, R., "Internal Hydrogen Embrittlement of Ultrahigh-Strength AERMET 100 Steel," *Metallurgical and Materials Transactions A: Physical Metallurgy and Materials Science*, Vol. 34, No. 2, 2003, pp. 327–344. doi:10.1007/s11661-003-0334-3

[10] Yuyama, T. S., Kishi, K., and Hisamatsu, Y., "Fundamental Aspects of AE Monitoring on Corrosion Fatigue Process in Austenitic Stainless Steel," *Journal of Materials for Energy Systems*, Vol. 5, No. 4, 1984, pp. 212–221.

[11] Rongsheng, G. "Modern Acoustic Emission Technique and Its Application in Aviation Industry," *Ultrasonics*, Vol. 44, 2006, pp. 1025–1029. doi:10.1016/j.ultras.2006.05.092

[12] Baxter, M., Pullin, R., Holford, L., and Evans, S., "Detection of Fatigue Crack Growth in Aircraft Landing Gear 4 Point bend Test Specimens," *Engineering Materials and Design*, Vols. 293–294, 2005, pp. 193–200.

[13] Harris, D., and Dunegan, H., "Continuous Monitoring of Fatigue-Crack Growth by Acoustic Emission Technique," *Experimental Mechanics*, Feb. 1974, pp. 70–81.

[14] *Non Destructive Testing Handbook*, 2nd ed., Vol. 5, American Society for Nondestructive Testing, Columbus, OH, 1987.

[15] Weng, C., Lin, G., and Chen, R. "Acoustic Emission Characterization of a Medium Strength Steel During Hydrogen Charging Processes," *Materials Science and Engineering*, Vol. A154, No. 1, 1992, pp. 52–57.

[16] Antolovich, S., "Fatigue Crack Propagation and Corrosion Fatigue of AF1410 Steel," Air Force Materials Laboratory: Air Force System Command, Ohio TR AFML-TR-79-4209, May 1978.

[17] Agarwala, V., "What's Eating Us: Corrosion," *Naval Research Reviews*, Vol. 50, No. 4, 1998, pp. 14–24.

[18] Olive, J., Cwiek, J., and Desjardins, D., "Quantification of the Hydrogen Produced During Corrosion Fatigue Crack Propagation," *Corrosion Science*, Vol. 41, No. 6, 1999, pp. 1067–1078. doi:10.1016/S0010-938X(98)00151-6

[19] Oriani, R., "The Diffusion and Trapping of Hydrogen in Steel," *Acta Metallurgica*, Vol. 18, No. 1, 1970, pp. 147–157. doi:10.1016/0001-6160(70)90078-7

[20] Quispitupa, A., Shafiq, B., Charca, S., Uwakweh, O., and Suarez, M., "Effect of Hydrogen and Hold Time on the Fatigue Lifetime of AF1410 Aircraft Structural Steel," *Journal of Aircraft*, Vol. 44, No. 2, 2007, pp. 453–458. doi:10.2514/1.23516

[21] Birnbaum, H., "Mechanisms of Hydrogen Related Fracture of Metals," *Proceedings of Fourth International Conference on the Effects of Hydrogen on the Materials Behavior*, edited by Neville R. Moody and Anthony E. Thompson, TMS Publications, Pittsburgh, PA, 1989, pp. 639–660.

[22] Ayer, R., and Machmeier, P., "Microstructural Basis for the Effect of Chromium on the Strength and Toughness of AF1410-Based High Performance Steel," *Metallurgical and Materials Transactions A: Physical Metallurgy and Materials Science*, Vol. 27A, No. 9, 1996, pp. 2510–2517. doi:10.1007/BF02652345

[23] Li, D., Gangloff, R., and Scully, J., "Hydrogen Trap States in Ultrahigh-Strength AERMET 100 Steel," *Metallurgical and Materials Transactions A: Physical Metallurgy and Materials Science*, Vol. 35A, No. 3, 2004, pp. 849–864. doi:10.1007/s11661-004-0011-1